Inorganic Chemistry
Article
Cite This: *Inorg. Chem.* XXXX, XXX, XXX−XXX
pubs.acs.org/IC

Intramolecular Hydrogen Bonding Facilitates Electrocatalytic Reduction of Nitrite in Aqueous Solutions

Song Xu,[†] Hyuk-Yong Kwon,[‡] Daniel C. Ashley,[‡] Chun-Hsing Chen,[†] Elena Jakubikova,*,[‡] and Jeremy M. Smith*,[†]

[†]Department of Chemistry, Indiana University, 800 East Kirkwood Avenue, Bloomington, Indiana 47401, United States
[‡]Department of Chemistry, North Carolina State University, 2620 Yarbrough Drive, Raleigh, North Carolina 27695, United States

Supporting Information

ABSTRACT: This work reports a combined experimental and computational mechanistic investigation into the electrocatalytic reduction of nitrite to ammonia by a cobalt macrocycle in an aqueous solution. In the presence of a nitrite substrate, the Co(III) precatalyst, $[Co(DIM)(NO_2)_2]^+$ (DIM = 2,3-dimethyl-1,4,8,11-tetraazacyclotetradeca-1,3-diene), is formed *in situ*. Cyclic voltammetry and density functional theory (DFT) calculations show that this complex is reduced by two electrons, the first of which is coupled with nitrite ligand loss, to provide the active catalyst. Experimental observations suggest that the key N−O bond cleavage step is facilitated by intramolecular proton transfer from an amine group of the macrocycle to a nitro ligand, as supported by modeling several potential reaction pathways with DFT. These results provide insights into how the combination of a redox active ligand and first-row transition metal can facilitate the multiproton/electron process of nitrite reduction.

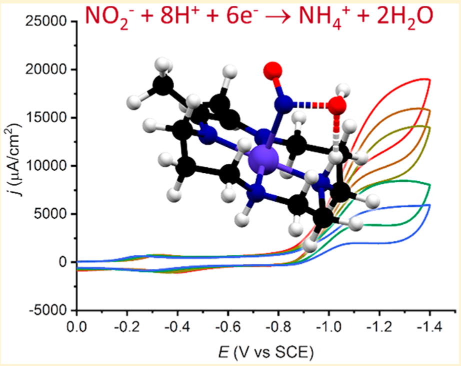

Largely as a consequence of the increased availability of ammonia through the Haber−Bosch process,[1] the scale of human intervention in the global nitrogen cycle is larger than that of any other basic element cycle, including carbon.[2] While fertilizers derived from Haber−Bosch ammonia are critical to feeding the planet, it is estimated that only 17% of the 135 million tons of agricultural nitrogen is retained as vegetable and meat protein,[3] with the remainder lost to the environment, including in the form of soluble and/or volatile nitrogen oxides.[4] The attendant nitrogen pollution has multiple adverse impacts, affecting both biodiversity[5] and human health,[6] and is associated with significant economic costs. For example, the total annual nitrogen-related damage in EU-27 has been estimated to be as much as 4% of the average European income.[7]

Nitrite is formed as an intermediate species in the biological nitrification process that converts ammonia to nitrate. Although the juxtaposition and coupled rates of ammonia oxidizing and nitrite oxidizing bacteria in terrestrial and aquatic ecosystems usually lead to low steady-state concentrations of nitrite, a number of environmental effects, e.g., low levels of dissolved oxygen, may lead to increased concentrations.[8] High nitrite concentrations are a serious water quality concern because of its high toxicity to humans, plants, and animals. For example, nitrite irreversibly oxidizes hemoglobin to methemoglobin, which compromises the oxygen binding capacity and leads to respiratory deficiencies.[8]

Because the massive influx of anthropogenic nitrogen overwhelms natural remediation processes, there is an opportunity to develop electrocatalysts that convert nitrite to more useful or benign forms. The electrocatalytic reduction of nitrite presents a number of challenges for catalyst design. First, nitrite has a complex aqueous phase chemistry and can access a number of different electroactive forms, with NO_2^- being dominant in alkaline and neutral solutions, HNO_2 in moderately acidic solutions, and NO^+ in highly acidic solutions. Nitrous acid also disproportionates to provide free NO and nitric acid in mildly acidic solutions.[9] Second, there are multiple possible reduction products that are thermodynamically favorable, some of which have undesirable properties, such as N_2O, a potent greenhouse gas.[10] Finally, intermediate species formed from partial reduction may react with nitrite to provide undesired products, particularly in acidic media, e.g., with NH_3OH^+ to give N_2O.

A number of molecular electrocatalysts for the reduction of aqueous nitrite have been reported.[11−18] Inspired by biological reduction of nitrite by heme-containing metalloenzymes (e.g., cytochrome *c* nitrite reductase),[19,20] the electrocatalytic reduction of nitrite by $[Fe^{III}(H_2O)(TPPS)]^{3-}$ [H_2TPPS^{4-} = tetraanionic form of *meso*-tetrakis(*p*-sulfonatophenyl)-porphyrin] has been investigated in some detail. While ammonia is the ultimate reduction product of electrocatalysis, hydroxylamine and nitrous oxide are significant side products, depending on the reaction conditions.[21] By contrast, iron-substituted polyoxotungstates produce only ammonia, which is

Received: May 1, 2019

DOI: 10.1021/acs.inorgchem.9b01274
Inorg. Chem. XXXX, XXX, XXX−XXX

Scheme 1

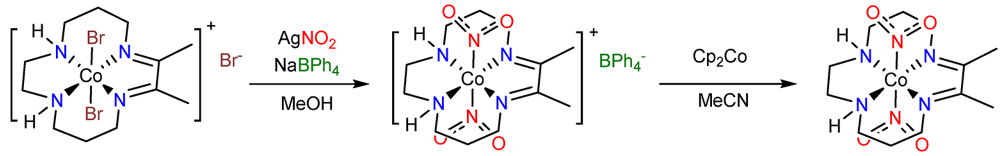

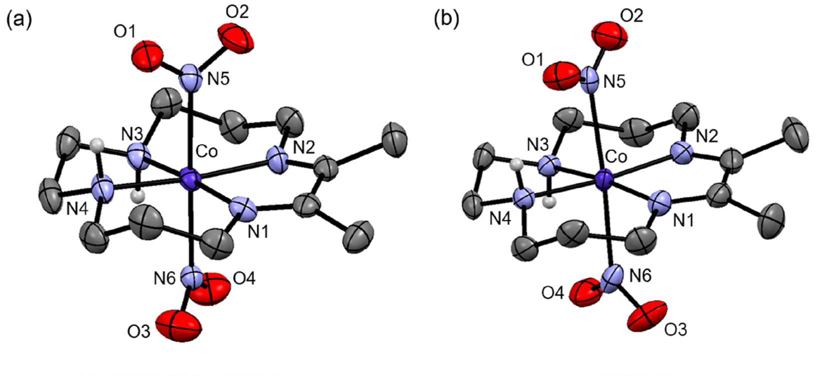

[Co(DIM)(NO$_2$)$_2$](BPh$_4$) **Co(DIM)(NO$_2$)$_2$**

Figure 1. Molecular structures of (a) [Co(DIM)(NO$_2$)$_2$]BPh$_4$ and (b) Co(DIM)(NO$_2$)$_2$ with 50% probability ellipsoids. The BPh$_4$ anion, solvent molecules, and most H atoms have been omitted for the sake of clarity.

Table 1. Selected Bond Lengths (angstroms) and Angles (degrees) of [Co(DIM)(NO$_2$)$_2$]$^+$ and Co(DIM)(NO$_2$)$_2$

	[Co(DIM)(NO$_2$)$_2$]$^+$ (experimental)	Co(DIM)(NO$_2$)$_2$ (experimental)	[Co(DIM)(NO$_2$)$_2$]$^+$ (calculated)	Co(DIM)(NO$_2$)$_2$ (calculated)
Co–N1	1.928(3)	1.918(3)	1.953	1.955
Co–N2	1.941(3)	1.925(3)	1.960	1.960
Co–N3	1.965(3)	1.984(3)	1.971	1.998
Co–N4	1.968(3)	1.986(3)	1.972	1.999
Co–N5	2.004(3)	2.306(3)	1.990	2.269
Co–N6	1.961(3)	2.289(3)	1.994	2.272
N5–Co–N6	178.8(1)	176.5(1)	179.3	175.3

proposed to be a consequence of the redox active polyoxometallate ligand's ability to store multiple electrons before they are simultaneously transferred to the bound substrate.[22] Despite differences in product distribution and reaction mechanism, the highly facile formation of a nitrosyl ligand is a common feature to both of these catalyst systems.[23] More recently, a CoGGH complex (GGH = Gly-Gly-His model tripeptide) was reported to electrocatalytically reduce nitrite to ammonium in aqueous solutions with nitric oxide and hydroxylamine proposed as intermediates.[18]

We previously reported an investigation into the mechanism of the reduction of nitrate to ammonia by the cobalt macrocycle electrocatalyst, [Co(DIM)]$^+$. This work demonstrated that the combination of redox activity and flexibility provided by the DIM macrocycle is critical to facilitating N–O bond cleavage of coordinated nitrate, which affords a nitrito complex with loss of water.[24] However, the subsequent reduction steps leading to the formation of ammonia were not investigated. In addition to being a catalyst for nitrate reduction, [Co(DIM)]$^+$ has also been shown to electrocatalytically reduce nitrite and hydroxylamine to ammonia;[25] however, little is known about the catalytic performance or reaction mechanism. In this paper, we present a combined experimental and computational investigation into the electrochemical reduction of nitrite by [Co(DIM)]$^+$. The insights from this study are also relevant to the mechanism by which [Co(DIM)]$^+$ catalyzes the eight-electron reduction of nitrate to ammonia.

RESULTS AND DISCUSSION

Synthesis and Characterization. Reaction of [Co(DIM)Br$_2$]Br with 3 equiv of AgNO$_2$ in MeOH, followed by 1 equiv of NaBPh$_4$, provides the diamagnetic complex [Co(DIM)(NO$_2$)$_2$]BPh$_4$ (Scheme 1). The molecular structure of [Co(DIM)(NO$_2$)$_2$]$^+$ was unambiguously confirmed by single-crystal X-ray diffraction (Figure 1a), which reveals the anticipated structure. Similar to previously reported [Co(DIM)Br$_2$]$^+$ and [Co(DIM)(NO$_3$)$_2$]$^+$,[24] the cobalt ion is coordinated by a square planar array of the four macrocycle N donors, with the two axial nitro ligands completing the coordination sphere. In contrast to its nitrate analogue, [Co(DIM)(NO$_3$)$_2$]$^+$,[24] the axial nitro ligands of [Co(DIM)(NO$_2$)$_2$]$^+$ bind to the Co center through N donors. Although intramolecular hydrogen bonding between oxygen atoms of the nitro ligand and amine protons of the DIM might be expected, the long O···H distance (~2.0 Å) suggests that this does not occur in the solid state.

As suggested by cyclic voltammetry (see below), [Co(DIM)(NO$_2$)$_2$]BPh$_4$ can be chemically reduced to the low-spin ($S = {}^1/_2$) Co(II) complex, Co(DIM)(NO$_2$)$_2$, by reaction with 1 equiv of cobaltocene (Cp$_2$Co) (Scheme 1). The molecular structure of Co(DIM)(NO$_2$)$_2$, as determined by single-crystal X-ray diffraction (Figure 1b), reveals the

DOI: 10.1021/acs.inorgchem.9b01274
Inorg. Chem. XXXX, XXX, XXX–XXX

anticipated structure with cobalt having the same coordination sphere as in the Co(III) analogue. While the Co−N(amine) and Co−N(imine) bond lengths do not show any dramatic changes, there is a significant elongation (~0.3 Å) of the Co−NO_2 bonds (Table 1), which can be attributed to the presence of an unpaired electron in the σ^* d_{z^2} orbital of low-spin Co(II). The magnetic susceptibility, as determined by the method of Evans (μ_{eff} = 1.73 μ_B), confirms the $S = {}^1/_2$ formulation. Density functional theory (DFT) calculations performed on the oxidized and reduced complexes show similar structural changes and also predict the ground state of the Co(II) complex to be a doublet.

Electrochemical Studies of $[(DIM)Co(NO_2)_2]^+$ in MeCN. Like $[Co(DIM)Br_2]^+$,[24] two reversible reductions are observed in the cyclic voltammogram (CV) of $[Co(DIM)(NO_2)_2]^+$ in acetonitrile, with $E_{1/2}$ values of −0.53 and −0.96 V versus SCE (Table 2, Figure 2, and Figure S6). These waves can be assigned in light of the assignments previously made for $[Co(DIM)Br_2]^+$. Thus, the first wave can be assigned to the Co(III)/Co(II) couple, which is cathodically shifted by 0.50 V with respect to the analogous process in $[Co(DIM)Br_2]^+$, consistent with nitrite being a stronger field ligand than bromide. The second process, which occurs at essentially the same potential as for $[Co(DIM)Br_2]^+$, can be assigned as a ligand-based reduction, i.e., Co(II)(DIM)/Co(II)($DIM^−$). Thus, $[Co(DIM)(NO_2)_2]^+$ has electrochemical properties similar to those of $[Co(DIM)Br_2]^+$ and can store two electrons, one on cobalt and one on the redox active macrocycle.

Table 2. Reduction Potentials ($E_{1/2}$) for $[Co(DIM)Br_2]^+$ and $[Co(DIM)(NO_2)_2]^+$ (vs SCE)

	Co(III)/Co(II)	Co(II)(DIM)/Co(II)($DIM^−$)
$[Co(DIM)Br_2]^+$	−0.03	−0.90
$[Co(DIM)(NO_2)_2]^+$	−0.53	−0.96
$\Delta E_{1/2}$	0.50	0.06

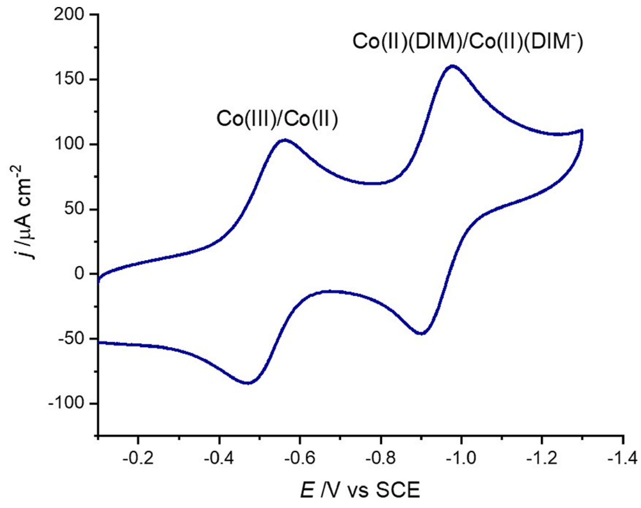

Figure 2. Cyclic voltammogram of $[Co(DIM)(NO_2)_2](BPh_4)$ in an acetonitrile solution. GC electrode, 100 mM NBu_4PF_6; scan rate, 100 mV/s.

Aqueous Speciation. While $[Co(DIM)(NO_2)_2]BPh_4$ is insoluble in water, $[Co(DIM)(NO_2)_2]^+$ can be generated *in situ* by adding 2 equiv of $NaNO_2$ to an aqueous solution of $[Co(DIM)Br_2]^+$, which is confirmed by ^1H nuclear magnetic resonance and ultraviolet−visible spectroscopy (Figures S5 and S7). It is also notable that there is no change in the pH for solutions of $[Co(DIM)(NO_2)_2]^+$, suggesting that there is little of the hydrolysis that is observed for aqueous solutions of $[Co(DIM)Br_2]^+$.

The CV of *in situ*-generated aqueous $[(DIM)Co(NO_2)_2]^+$ reveals a reversible anodic wave at approximately −0.3 V versus SCE that is assigned to the Co(III)/Co(II) couple (Figure 3a). As the $NO_2^−$ concentration is increased, the $E_{1/2}$ of the wave shifts to more negative potentials, with a dependence of −77 mV/log[$NO_2^−$] (Figure 3b). The observed dependence of $E_{1/2}$ on [$NO_2^−$] is consistent with nitrite ligand dissociation being coupled to electron transfer (Scheme 2), as determined by the following equation, which is derived from the Nernst equation under equilibrium conditions:

$$\Delta E_{1/2} = \frac{RT}{nF}\ln([NO_2^-])$$

Because the concentration of $[(DIM)CoBr_2]^+$ is kept constant at 0.5 mM for each measurement, $\Delta E_{1/2}$ does not depend on the concentration of any of the Co species. The difference between the theoretically expected slope (−59 mV/log[$NO_2^−$]) and the experimentally observed slope (−77 mV/log[$NO_2^−$]) may be due to additional equilibria involving loss of a second $NO_2^−$ ligand. Nonetheless, the loss of one $NO_2^−$ accounts for the bulk of the observed behavior. The $[Co(DIM)(NO_2)_2]^+/[Co(DIM)NO_2]^+$ reduction potential under standard conditions, E^0 of Scheme 2, is obtained from the intercept of the plot in Figure 3b (E^0 = −0.37 V vs SCE). The experimental conclusions are consistent with those obtained from calculations as discussed below.

Computed Aqueous Speciation. DFT calculations were used to further explore the speciation of $[Co(DIM)(NO_2)_2]^+$ in aqueous solutions. Previous work on $[Co(DIM)(NO_3)_2]^+$ and $[Co(DIM)Br_2]^+$ was able to reasonably reproduce the experimentally observed hydrolysis and subsequent deprotonation of the complexes. For the case of $[Co(DIM)(NO_2)_2]^+$, the calculated binding free energies of nitrite (see Scheme 3) are quite large, 19.5 and 13.0 kcal/mol for the first and second nitrite ligand, respectively. These values are ~7 kcal/mol more favorable for the analogous reactions with bromide loss as reported previously.[24] Even upon addition of subsequent binding of a water ligand, which is favorable (−6.6 kcal/mol), it is far too energetically uphill (12.9 kcal/mol) to replace the nitrite ligand. This is consistent with the experimental observation that there is no change in pH upon formation of $[Co(DIM)(NO_2)_2]^+$ *in situ*.

The calculated standard reduction potential of $[Co(DIM)(NO_2)_2]^+$ is −0.23 V versus SCE, which agrees well with the observed reduction at −0.37 V. This level of error is similar to what has been seen for this computational methodology when used to calculate other experimentally known Co(III)/Co(II) reduction potentials.[24] While the loss of nitrite from $[Co(DIM)(NO_2)_2]^+$ is thermodynamically uphill by 19.5 kcal/mol, it is only −3.6 and 3.8 kcal/mol to lose the first and second nitrite ligands for the reduced $Co(DIM)(NO_2)_2$ complex, respectively, which is consistent with the nitrite loss being coupled to the reduction.

As shown in Scheme 3, the calculated reduction potentials of the Co(II) complex vary from −1.57 to −1.21 V depending on the number of nitrites bound. In the previous study of nitrate reduction, the doubly reduced $[Co(DIM)(NO_3)_2]^−$ complex could not be calculated, but here, we do note that when only

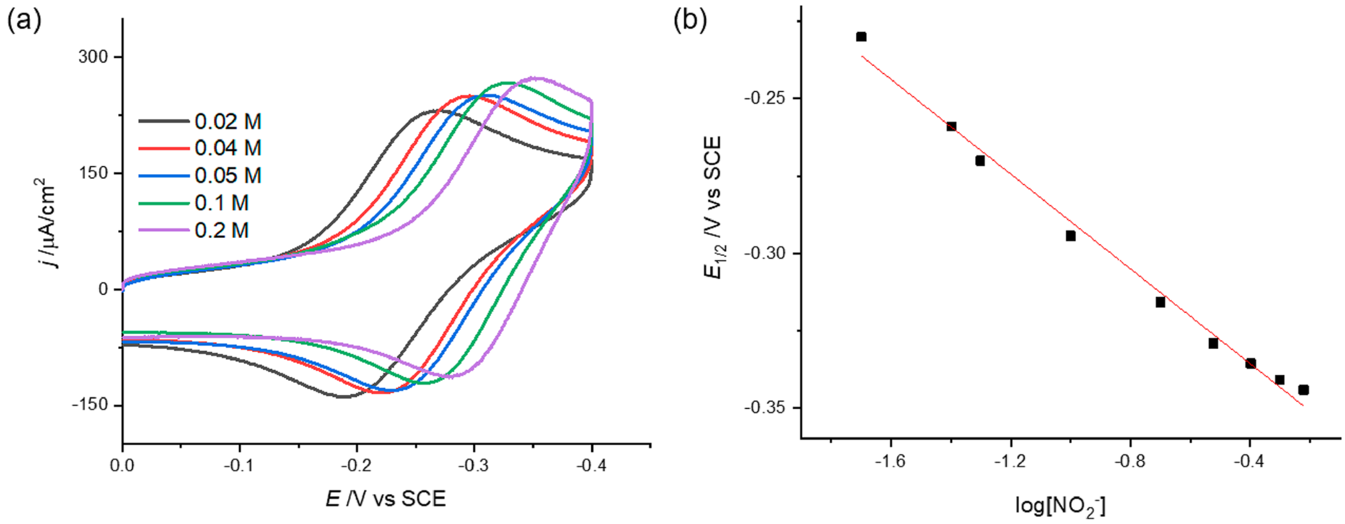

Figure 3. (a) Selected cyclic voltammograms of 0.5 mM $[(DIM)CoBr_2]^+$ with different concentrations of $NaNO_2$ (scan rate = 500 mV/s, glassy carbon working electrode, pH = 6.0, 100 mM Na_2SO_4. (b) Plot of $E_{1/2}$ vs $\log[NO_2^-]$, where $E_{1/2}$ values are calculated from cyclic voltammograms and $[NO_2^-]$ is the concentration of $NaNO_2$ in solution. The plot fits the equation $y = -0.077x - 0.37$ ($R^2 = 0.991$).

Scheme 2. Proposed Redox-Coupled Binding of a Nitrite Ligand

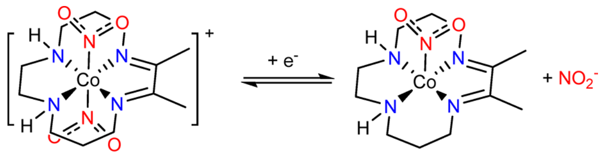

one anion is bound the calculated ligand-based reduction potential for $[Co(DIM)(NO_3)]^+$ (−1.35 V) was virtually identical to that of $[Co(DIM)(NO_2)]^+$ (−1.40 V). While these are more negative than the onset of the catalytic wave (see below), the previous computational work suggested that the favorability of ligand-based reductions was underestimated by the chosen computational methodology. Moreover, the fact that the nitrite and nitrate Co(II) complexes show similar

Scheme 3. Computational Square Scheme Generated by DFT Calculations[a]

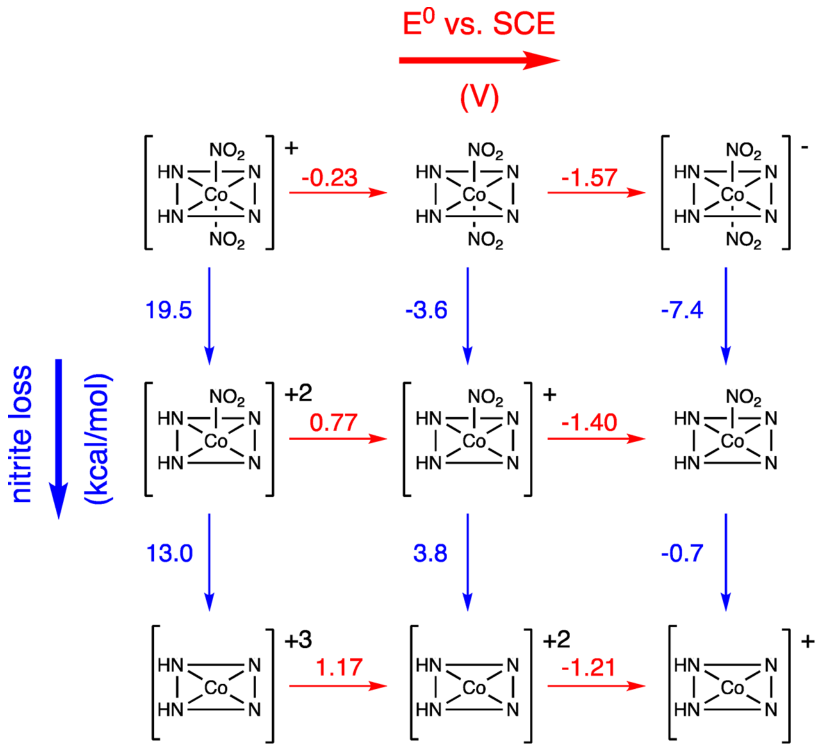

[a]Horizontal pathways represent calculated one-electron reduction potentials and are reported in volts vs SCE. Vertical pathways represent dissociation of nitrite and are reported in kcal/mol. See Figure S22 for additional square schemes. The values given in these schemes are calculated using the lowest-energy spin state and binding mode of nitrite (N-bound vs O-bound) for each complex. A more detailed version of this scheme indicating spin states and nitrite binding modes is provided as Figure S23.

calculated reduction potentials for the ligand-based reduction agrees with the similar experimental behavior of the second reduction of the nitrite and nitrate Co(III) complexes (Table 2). Finally, the Co(I) complex is predicted to reversibly bind a single nitrite ligand, and this complex can then serve as the starting point for mechanistic investigations.

Electrocatalytic NO_2^- Reduction. A catalytic current attributed to NO_2^- reduction is observed with an onset potential of approximately −0.9 V versus SCE in the CV of 0.5 mM $[Co(DIM)Br_2]^+$ in the presence of 10 mM aqueous nitrite. The observed onset potential is almost identical to that observed for the electrocatalytic reduction of aqueous nitrate under the same conditions, suggesting that nitrite reduction is initiated by a similar electrochemical process as for nitrate reduction. Despite their similar reduction potentials, the peak current density for electrocatalytic nitrite reduction is almost 10-fold larger than for nitrate reduction, indicating faster catalysis (Figure S10).

To characterize the nature of the nitrite reduction products, a 0.1 M solution of $NaNO_2$ in the presence of 0.5 mM $[Co(DIM)Br_2]^+$ (initial pH of 7.2) was subject to controlled potential electrolysis (CPE) at −1.05 V versus SCE for 2 h, providing ammonia as the sole nitrogen-containing product in 88% Faradaic efficiency. It is noteworthy that no hydroxylamine and ammonia were detected in the solution following CPE of 0.5 mM $[Co(DIM)Br_2]^+$ in the absence of $NaNO_2$, indicating that the NH_3 originates from NO_2^- rather than the N atoms of the DIM ligand (Figure S11).

The electrocatalytic performance of $[Co(DIM)Br_2]^+$ compares favorably with those of most previously investigated electrocatalysts for aqueous nitrite reduction in aqueous solutions. For example, $[Fe^{III}(H_2O)(TPPS)]^{3-}$ reduces nitrite with an onset potential of approximately −0.5 V versus SCE; however, the product distribution is sensitive to the applied potential, with more negative potentials favoring ammonia formation.[21] By contrast, iron-substituted polyoxotungstates produce ammonia as the only nitrogen-containing product with an onset potential of approximately −0.7 V versus SCE; however, the Faradaic efficiency is low.[22] More recently, a cobalt−tripeptide complex with an onset potential of approximately −0.65 V versus SCE for nitrite reduction has been reported. This catalyst also reduces nitrite to ammonia (3×10^3 turnovers over 5.5 h at −0.90 vs SCE at pH 7.2) in a noncoordinating aqueous buffer using Hg as the working electrode.[18] Other electrocatalysts are limited by poor product selectivity, the need for basic conditions, or both.[12−17]

Mechanistic Investigations. The catalytic current for nitrite reduction shows an S-shaped response at scan rates of >3 V/s, which indicates homogeneous electrocatalysis under pure kinetic conditions (Figure S13).[26,27] Under these conditions, catalytic plateau current i_c is described by

$$i_c = nFAC_P\sqrt{DkC_A}$$

where k is the rate constant of NO_2^- reduction, C_P is the bulk concentration of $[Co(DIM)Br_2]^+$, and C_A is the bulk concentration of NO_2^-. The reduction of nitrite to ammonia requires six electrons ($n = 6$). The current dependence under pure kinetic conditions revealed first-order dependencies on the concentration of the catalyst $\{[Co(DIM)Br_2]^+\}$ and the substrate ($NaNO_2$), consistent with the second-order rate law: rate = $k[Co][NO_2]$, where $k = (5.9 \pm 0.4) \times 10^3\ M^{-1}\ s^{-1}$ at 298 K,[28] with turnover frequency 118 s^{-1}.[29] Similarly to electrocatalytic NO_3^- reduction, the plateau current density is pH-independent (Figure 4c),[30] suggesting that proton transfer occurs after the rate-determining step.

Analysis of the temperature dependence of the catalytic current gives activation parameters for the reaction: $\Delta H^\ddagger = 7.3 \pm 0.5$ kcal/mol, and $\Delta S^\ddagger = -14 \pm 2$ e.u. (Figure S15). Although there is no proton dependence in the rate law, a kinetic isotope effect $[k_{cat,H}/k_{cat,D} = (i_{cat,H}/i_{cat,D})^2 = 2.6]$ is obtained from the relative catalytic currents observed in H_2O and D_2O (Figure S16).[31] This apparent contradiction can be reconciled by the suggestion that intramolecular hydrogen bonding is critical to nitrite reduction. Specifically, because the macrocycle amine protons are exchanged for deuterium in deuterated solvents[24] (see also Figure S17), a kinetic isotope effect is expected if N−O bond cleavage is assisted by the N−H groups of the DIM ligand, even if the rate law does not show a proton dependence.

Mechanistic Investigation Using Density Functional Theory. To further investigate the mechanism for nitrite reduction with $[Co(DIM)]^+$ as an active catalyst, DFT calculations were performed using B3LYP[32−34]+D2[35] with the SDD on the Co[36,37] and 6-311+G**[38,39] basis set on all other atoms in solution (for details, see the Supporting Information). The ground-state electronic structure for $[Co(DIM)]^+$ was previously described as an antiferromagnetically coupled triplet (AF-T) in which a π-conjugated orbital of the DIM ligand is coupled with a d orbital of cobalt, ultimately yielding approximately one unpaired electron on DIM of opposite spin to approximately three unpaired electrons on the metal center.[24] Although formally $[Co(DIM)]^+$ is a Co(I) complex, due to this complex electronic structure it is better described as a Co(II)-DIM(-I) species. While the end product of the reduction of nitrite is ultimately ammonia,[25] only the initial step, the formation of a nitrosyl ligand, is discussed here. The nitrosyl to ammonia conversion is a nontrivial multistep process that involves five protons and four electrons; hence, we intend to discuss it in detail in future work. Several simple but plausible mechanisms of nitrite reduction with $[Co(DIM)]^+$ as the active catalyst were investigated.

The first step of each mechanism involves binding of nitrite to cobalt. It is possible that a nitrite ligand stays bound from the initially formed Co(III) complex all the way to the Co(I) state and then begins the reaction cycle, but it is also possible that nitrite loss and rebinding may occur along the way on the basis of the relatively small binding energies for binding of nitrite to four-coordinate Co-DIM when the complex is formally Co(I) and Co(II) {binding is −3.8 kcal/mol for $[Co(II)\text{-}DIM]^{2+}$ and 0.7 kcal/mol for $[Co(I)\text{-}DIM]^+$}. Therefore, it is appropriate to begin the mechanistic discussion by accounting for the possibility of nitrite binding.

Nitrite can bind to cobalt through either the nitrogen atom or the oxygen atom. Binding through either atom is feasible with only a small energy difference between the two: 1.5 kcal/mol to form the nitro complex (**2**) and 0.7 kcal/mol to form the nitrito complex (**6**) with activation barriers of 5.4 and 5.6 kcal/mol, respectively. While both binding modes are similar in energy, protonation is 3.8 kcal/mol more favorable for the nitro-bound structure, and hence, the nitrito ligand shifts to a nitro ligand after a protonation step through a bidentate intermediate (**10**) as illustrated in Figure 5.

Note that an N−O bond must be broken to form the O-bound or N-bound nitrosyl complex. The N−O bond is harder to break for the O-bound nitrosyl complex because the

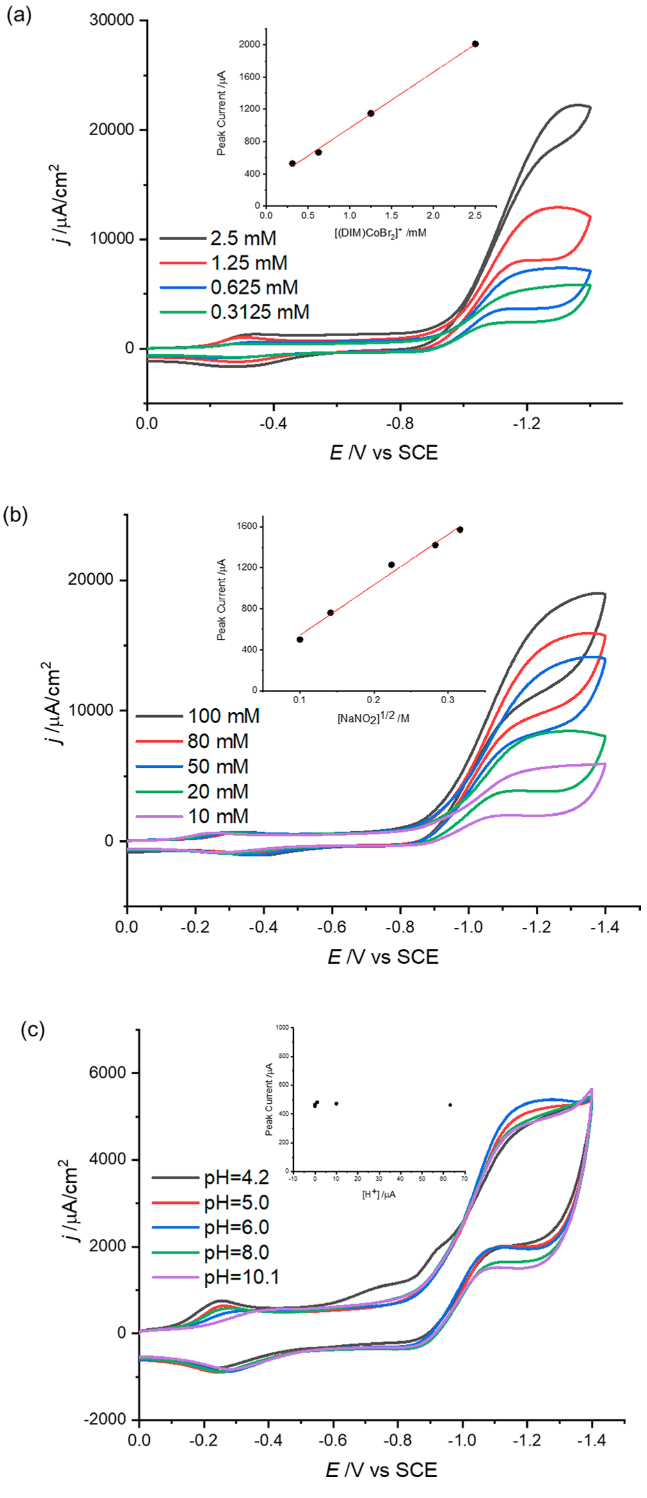

Figure 4. (a) Cyclic voltammograms of 20 mM $NaNO_2$ with different concentrations of $[Co(DIM)Br_2]^+$ at pH 6.0. (b) Cyclic voltammograms of 0.5 mM $[Co(DIM)Br_2]^+$ with different concentrations of $NaNO_2$ at pH 6.0. (c) Cyclic voltammograms of 0.5 mM $[Co(DIM)Br_2]^+$ with 10 mM $NaNO_2$ at different pH values. GC electrode, scan rate of 3 V/s, electrolyte of 100 mM Na_2SO_4. Insets show dependence of peak current on concentration. The inset of panel b is a plot of NO_2^- concentration vs peak current. The inset of panel c is a plot of H^+ concentration vs peak current.

resulting Co—O═N complex is less stable than the Co—N═O complex. More detailed mechanistic pathways for the O-bound complex are presented in the Supporting Information.

Once **2** is formed, the nitro ligand will be spontaneously protonated when the pH is below 11.7. Bound nitrous acid is a better oxidant than the nitro ligand; protonation will induce transfer of the unpaired electron on DIM directly to a π^* orbital of nitrous acid (**3**). As electron spin changes from AF-T in **3** to AF-S in **13**, the nitrogen atom becomes pyramidalized (Figure 7 and Figures S20 and S21).

While direct heterolytic cleavage of the N—OH bond in **13** to form free hydroxide is unlikely to happen (>20 kcal/mol), hydroxyl can migrate either to an sp^2 carbon on DIM [ligand-mediated mechanism (blue in Figure 6)] or to cobalt [hydroxyl transfer mechanism (red in Figure 6)]. The activation energy and the driving force for the N—O cleavage step are similar for both of these pathways as shown in the reaction coordinate diagram (Figure 6). However, the ligand-mediated mechanism eventually has to overcome an energy barrier of 48.2 kcal/mol after another protonation step to complete the cycle, so this mechanism is less plausible compared to the other explored mechanisms. However, it is worth noting that the barrier involved in the initial transfer of hydroxyl to the ligand is quite low, at only 8.9 kcal/mol, suggesting that this may be a potential degradation pathway during catalysis.

From **13** to **17**, the N—O bond breaks to form a six-coordinate complex with a metal-bound hydroxide and anionic nitrosyl six-coordinated complex. This step is downhill by −2.5 kcal/mol with an activation barrier of 8.6 kcal/mol. The nitrosyl complex (**18**) is finally obtained after loss of hydroxide that is downhill by −13.8 kcal/mol. The resulting nitrosyl ligand is best described as NO$^-$ based on the bent Co—N═O angle of 124.6°, suggesting that **18** is now formally Co(III), or $\{Co(NO)\}^8$.[40] Unlike the ligand-mediated mechanism, the hydroxyl transfer mechanism is still energetically feasible given that this final step has a reasonable activation energy of 12.2 kcal/mol (the **13**−**17** transition-state energy relative to complex **3**).

The last reaction pathway explored is the amino proton-assisted mechanism, which occurs through rotation of the HNO_2 ligand in **3** to orient the hydroxyl group toward one of the amino protons on DIM (**4**). The change in spin state from the AF triplet to the AF singlet (**4** to **5**) causes the nitro ligand to pyramidalize due to changes in the Co orbitals involved in AF coupling (see Figure 7 and Figure S21 and its accompanying discussion). The barrier for this process is approximated by an energetically accessible MECP that is only 5.5 kcal/mol higher than **4**. Intermediate **5** has a N—OH distance of 1.711 Å and an O—HN distance of 1.786 Å, suggesting that it possesses a hydroxide ion that is weakly bonded to both nitrosyl and the amino proton. Transfer of the amino proton to form a loosely bound water molecule (**11**) is facile. The free energy of activation is actually slightly negative. This "nonphysical" result arises only because the structures are necessarily optimized on the electronic energy surface, where the transition state is appropriately higher in energy than the reactants by 1.1 kcal/mol. Inclusion of thermochemical corrections (ZPE and entropy) results in the "negative" energy. The important result for this process is that this step is essentially barrierless. After the water molecule leaves, reprotonation of the DIM ligand from the solvent is downhill by −23.7 kcal/mol, which produces Co(III)—NO complex **18**. Overall, the activation barrier for the amino proton-assisted mechanism is 6.6 kcal/mol (the **4**−**5** MECP energy relative to

DOI: 10.1021/acs.inorgchem.9b01274
Inorg. Chem. XXXX, XXX, XXX−XXX

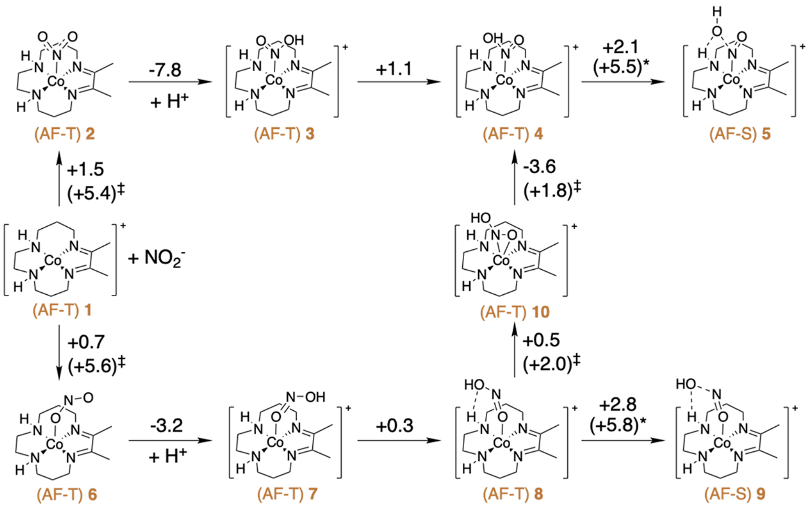

Figure 5. N-Bound and O-bound amino proton-asssisted mechanism energy comparison at pH 6 (ΔG is reported in kcal/mol). MECP energies are denoted with an asterisk.

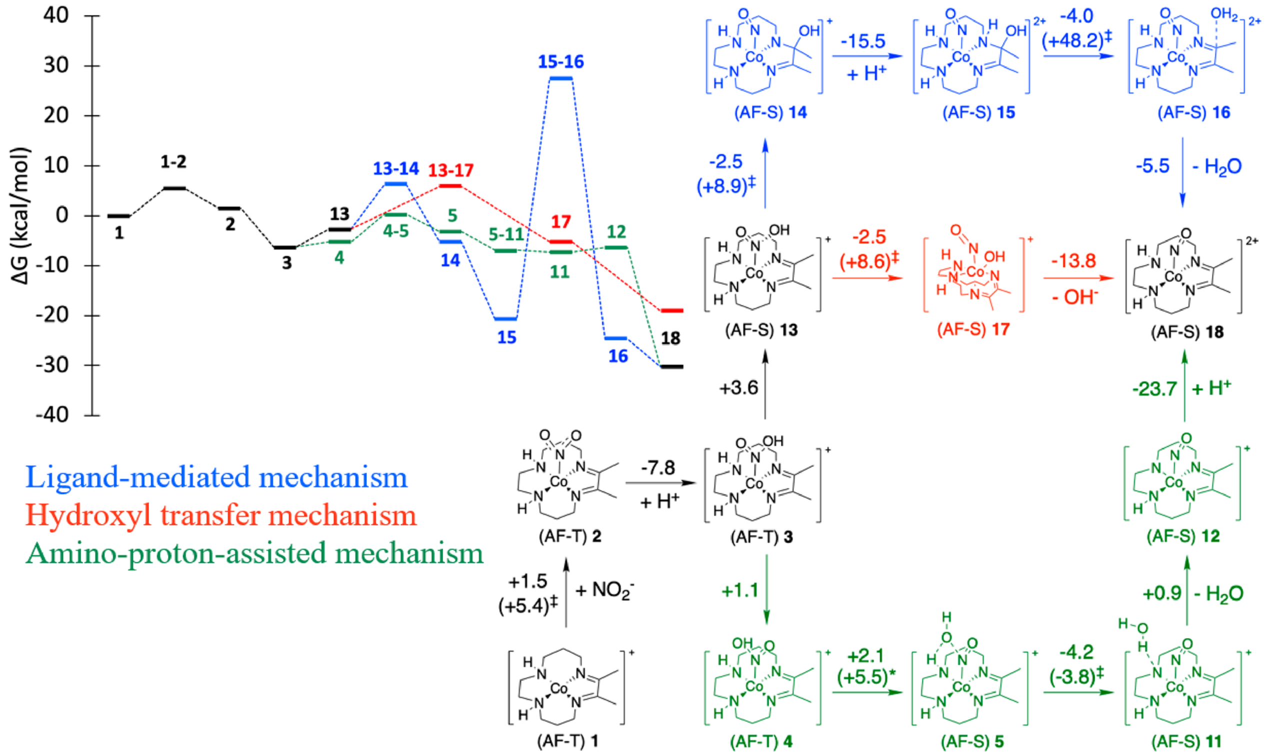

Figure 6. Nitrite reduction mechanisms examined with DFT and their corresponding reaction coordinate diagrams: ligand-mediated mechanism (blue), hydroxyl transfer mechanism (red), and amino proton-assisted mechanism (green). The energy of the minimum energy crossing point (MECP) is denoted with an asterisk. All reported energies are solvated ΔG values adjusted to pH 6 and given in kcal/mol.

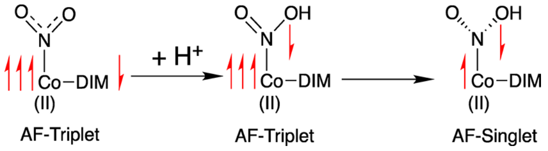

Figure 7. Illustration of relevant spin states along the reaction coordinate.

complex **3**), which is the lowest among those of the investigated mechanisms.

It is important to note that the energies discussed above were calculated assuming standard conditions of 1 M concentrations for all species involved. Changing the concentration of these species to 1 mM, which is more realistic compared to experiment, causes the barrier and driving force for nitrite binding to increase by 4.1 kcal/mol, which will make this step rate-determining with a 9.5 kcal/mol barrier. Note that this concentration dependence will occur for only a bimolecular reaction and hence affects nitrite binding but not the unimolecular MECP that was assigned as rate-determining for the amino proton-assisted mechanism above. Therefore, at low nitrite concentrations, the computational results agree with the electrochemistry data as they both suggest the reaction rate is linearly dependent on the concentration of the nitrite and Co catalyst, and independent of pH. In addition, this mechanism is consistent with the experimentally observed KIE, as proton transfer occurs intramolecularly from the amine group of the DIM ligand.

SUMMARY AND CONCLUSIONS

This work provides mechanistic insights into the electrocatalytic reduction of nitrite by $[Co(DIM)Br_2]^+$. In contrast to our work on the electrocatalytic reduction of nitrate,[24] which revealed complex aqueous speciation for $[Co(DIM)Br_2]^+$, use of the stronger field nitrite ligand results in six-coordinate complex $[Co(DIM)(NO_2)_2]^+$ being the only species observed in aqueous solutions. One-electron reduction of this complex is coupled to the loss of an axial nitrite ligand. An additional single-electron reduction leads to the formally Co(I) active catalyst that is better described as Co(II)-DIM(-I) according to the electronic structure calculations, which can reversibly bind nitrite. Thus, despite the stronger metal−ligand bond formed with nitrite, the active catalyst is similar to that previously proposed for nitrate reduction. However, in contrast to this earlier work, our investigations here reveal the critical importance of the macrocycle N−H groups to electrocatalysis. Specifically, intramolecular proton transfer facilitates N−O bond cleavage of the nitro ligand to provide a $\{CoNO\}^8$ intermediate along with H_2O. This proposal is supported by both DFT calculations and the experimentally determined deuterium KIE. Complexes with redox active ligands and/or proton shuttles have likewise been recently reported to facilitate both homogeneous stoichiometric and catalytic nitrite reduction.[11,41−44] Proton donor residue shuttles have also been proposed to play a key role in directing the mode of nitrite binding in myoglobin[45] as well as in the reduction of nitrite by cytochrome *c* nitrite reductatse (C*c*NiR).[20]

In summary, in addition to the previously reported features, such as the structural flexibility and redox non-innocence of the macrocycle,[24] the mechanistic insights obtained from this work reveal the importance of second-coordination sphere proton shuttles for the electrocatalytic reduction of nitrite. We anticipate that ongoing mechanistic investigations into electrocatalytic nitric oxide and hydroxylamine reduction will provide additional insights into the design of effective electrocatalysts for the reduction of nitrogen oxyanions.

ASSOCIATED CONTENT

Supporting Information

The Supporting Information is available free of charge on the ACS Publications website at DOI: 10.1021/acs.inorgchem.9b01274.

Additional data (XYZ)

Additional experimental and computational data (PDF)

Accession Codes

CCDC 1913290−1913291 contain the supplementary crystallographic data for this paper. These data can be obtained free of charge via www.ccdc.cam.ac.uk/data_request/cif, or by emailing data_request@ccdc.cam.ac.uk, or by contacting The Cambridge Crystallographic Data Centre, 12 Union Road, Cambridge CB2 1EZ, UK; fax: +44 1223 336033.

AUTHOR INFORMATION

Corresponding Authors

*E-mail: ejakubi@ncsu.edu.
*E-mail: smith962@indiana.edu.

ORCID

Daniel C. Ashley: 0000-0002-8838-4269
Elena Jakubikova: 0000-0001-7124-8300
Jeremy M. Smith: 0000-0002-3206-4725

Notes

The authors declare no competing financial interest.

ACKNOWLEDGMENTS

The authors thank the National Science Foundation for financial support (CHE-1566258).

REFERENCES

(1) Galloway, J. N.; Leach, A. M.; Bleeker, A.; Erisman, J. W. A chronology of human understanding of the nitrogen cycle. *Philos. Trans. R. Soc., B* **2013**, *368*, 20130120.

(2) Galloway, J. N.; Townsend, A. R.; Erisman, J. W.; Bekunda, M.; Cai, Z.; Freney, J. R.; Martinelli, L. A.; Seitzinger, S. P.; Sutton, M. A. Transformation of the Nitrogen Cycle: Recent Trends, Questions, and Potential Solutions. *Science* **2008**, *320*, 889.

(3) Matassa, S.; Batstone, D. J.; Hülsen, T.; Schnoor, J.; Verstraete, W. Can Direct Conversion of Used Nitrogen to New Feed and Protein Help Feed the World? *Environ. Sci. Technol.* **2015**, *49*, 5247.

(4) Fowler, D.; Coyle, M.; Skiba, U.; Sutton, M. A.; Cape, J. N.; Reis, S.; Sheppard, L. J.; Jenkins, A.; Grizzetti, B.; Galloway, J. N.; Vitousek, P.; Leach, A.; Bouwman, A. F.; Butterbach-Bahl, K.; Dentener, F.; Stevenson, D.; Amann, M.; Voss, M. The global nitrogen cycle in the twenty-first century. *Philos. Trans. R. Soc., B* **2013**, *368*, 20130164.

(5) Hernández, D. L.; Vallano, D. M.; Zavaleta, E. S.; Tzankova, Z.; Pasari, J. R.; Weiss, S.; Selmants, P. C.; Morozumi, C. Nitrogen Pollution Is Linked to US Listed Species Declines. *BioScience* **2016**, *66*, 213.

(6) Mensinga, T. T.; Speijers, G. J. A.; Meulenbelt, J. Health Implications of Exposure to Environmental Nitrogenous Compounds. *Toxicol. Rev.* **2003**, *22*, 41.

(7) Brink, C.; van Grinsven, H.; Jacobsen, B. H.; Rabl, A.; Gren, I.-M.; Holland, M.; Klimont, Z.; Hicks, K.; Brouwer, R.; Dickens, R.; Willems, J.; Termansen, M.; Velthof, G.; Alkemade, R.; van Oorschot, M.; Webb, J. Cost and Benefits of Nitrogen in the Environment. In *European Nitrogen Assessment*; Sutton, M. A., Howard, C. M., Erisman, J. W., Billen, G., Bleeker, A., Grennelt, P., van Grinsven, H., Grizzetti, B., Eds.; Cambridge University Press: Cambridge, U.K., 2011; Chapter 22.

(8) Philips, S.; Laanbroek, H. J.; Verstraete, W. Origin, causes and effects of increased nitrite concentrations in aquatic environments. *Rev. Environ. Sci. Bio/Technol.* **2002**, *1*, 115.

(9) Greenwood, N. N.; Earnshaw, A. In *Chemistry of the Elements*, 2nd ed.; Butterworth-Heinemann: Oxford, U.K., 1997; pp 406.

(10) Ravishankara, A. R.; Daniel, J. S.; Portmann, R. W. Nitrous Oxide (N_2O): The Dominant Ozone-Depleting Substance Emitted in the 21st Century. *Science* **2009**, *326*, 123.

(11) Timmons, A. J.; Symes, M. D. Converting between the oxides of nitrogen using metal-ligand coordination complexes. *Chem. Soc. Rev.* **2015**, *44*, 6708.

(12) Kuwabata, S.; Uezumi, S.; Tanaka, K.; Tanaka, T. Assimilatory and dissimilatory reduction of nitrate and nitrite with a tris(tetrabutylammonium) nonakis(benzenethiolato)octasulfidohexaferratedimolybdate(3-) modified glassy-carbon electrode in water. *Inorg. Chem.* **1986**, *25*, 3018.

(13) Taniguchi, I.; Nakashima, N.; Matsushita, K.; Yasukouchi, K. Electrocatalytic reduction of nitrate and nitrite to hydroxylamine and ammonia using metal cyclams. *J. Electroanal. Chem. Interfacial Electrochem.* **1987**, *224*, 199.

(14) Rhodes, M. R.; Barley, M. H.; Meyer, T. J. Electrocatalytic reduction of nitrite ion by edta complexes of iron(II) and ruthenium(II). *Inorg. Chem.* **1991**, *30*, 629.

(15) Zhang, J.; Lever, A. B. P.; Pietro, W. J. Electrochemical reduction of nitrite and nitric oxide catalyzed by an iron-alizarin

complexone adsorbed on a graphite electrode. *Inorg. Chem.* **1994**, *33*, 1392.

(16) Cheng, S.-H.; Su, Y. O. Electrocatalysis of Nitric Oxide Reduction by Water-Soluble Cobalt Porphyrin. Spectral and Electrochemical Studies. *Inorg. Chem.* **1994**, *33*, 5847.

(17) Chebotareva, N.; Nyokong, T. Metallophthalocyanine catalysed electroreduction of nitrate and nitrite ions in alkaline media. *J. Appl. Electrochem.* **1997**, *27*, 975.

(18) Guo, Y.; Stroka, J. R.; Kandemir, B.; Dickerson, C. E.; Bren, K. L. Cobalt Metallopeptide Electrocatalyst for the Selective Reduction of Nitrite to Ammonium. *J. Am. Chem. Soc.* **2018**, *140*, 16888.

(19) Fritz, G.; Einsle, O.; Rudolf, M.; Schiffer, A.; Kroneck, P. M. H. Key Bacterial Multi-Centered Metal Enzymes Involved in Nitrate and Sulfate Respiration. *J. Mol. Microbiol. Biotechnol.* **2006**, *10*, 223.

(20) Bykov, D.; Neese, F. Six-Electron Reduction of Nitrite to Ammonia by Cytochrome c Nitrite Reductase: Insights from Density Functional Theory Studies. *Inorg. Chem.* **2015**, *54*, 9303.

(21) Barley, M. H.; Meyer, T. J. Electrocatalytic reduction of nitrite to ammonia based on a water-soluble iron porphyrin. *J. Am. Chem. Soc.* **1986**, *108*, 5876.

(22) Toth, J. E.; Anson, F. C. Electrocatalytic reduction of nitrite and nitric oxide to ammonia with iron-substituted polyoxotungstates. *J. Am. Chem. Soc.* **1989**, *111*, 2444.

(23) Murphy, W. R.; Takeuchi, K.; Barley, M. H.; Meyer, T. J. Mechanism of reduction of bound nitrite to ammonia. *Inorg. Chem.* **1986**, *25*, 1041.

(24) Xu, S.; Ashley, D. C.; Kwon, H.-Y.; Ware, G. R.; Chen, C.-H.; Losovyj, Y.; Gao, X.; Jakubikova, E.; Smith, J. M. A flexible, redox-active macrocycle enables the electrocatalytic reduction of nitrate to ammonia by a cobalt complex. *Chem. Sci.* **2018**, *9*, 4950.

(25) Xiang, Y.; Zhou, D.-L.; Rusling, J. F. Electrochemical conversion of nitrate to ammonia in water using cobalt-DIM as catalyst. *J. Electroanal. Chem.* **1997**, *424*, 1.

(26) Savéant, J.-M. Molecular Catalysis of Electrochemical Reactions. Mechanistic Aspects. *Chem. Rev.* **2008**, *108*, 2348.

(27) Rountree, E. S.; McCarthy, B. D.; Eisenhart, T. T.; Dempsey, J. L. Evaluation of Homogeneous Electrocatalysts by Cyclic Voltammetry. *Inorg. Chem.* **2014**, *53*, 9983.

(28) See the Supporting Information for detailed rate constant calculations.

(29) The rate is faster than that suggested by the CPE results, presumably due to differences in experimental conditions. The CPE experiment was conducted at a less negative potential. Additionally, due to the lack of buffer in solution, the CPE experiments cannot be conducted at constant pH.

(30) At pH <4.0, a wave is observed at $E_{pc} = -0.8$ V versus SCE prior to that for nitrite reduction. This wave is tentatively proposed to arise from proton reduction. See Figure S14 for the CV response under more acidic conditions.

(31) Han, Y.; Wu, Y.; Lai, W.; Cao, R. Electrocatalytic Water Oxidation by a Water-Soluble Nickel Porphyrin Complex at Neutral pH with Low Overpotential. *Inorg. Chem.* **2015**, *54*, 5604.

(32) Becke, A. D. Density-functional exchange-energy approximation with correct asymptotic behavior. *Phys. Rev. A: At., Mol., Opt. Phys.* **1988**, *38*, 3098.

(33) Lee, C.; Yang, W.; Parr, R. G. Development of the Colle-Salvetti correlation-energy formula into a functional of the electron density. *Phys. Rev. B: Condens. Matter Mater. Phys.* **1988**, *37*, 785.

(34) Becke, A. D. Density functional thermochemistry. III. The role of exact exchange. *J. Chem. Phys.* **1993**, *98*, 5648.

(35) Grimme, S. Semiempirical GGA-type density functional constructed with a long-range dispersion correction. *J. Comput. Chem.* **2006**, *27*, 1787.

(36) Dolg, M.; Wedig, U.; Stoll, H.; Preuss, H. Energy adjusted ab initio pseudopotentials for the first row transition elements. *J. Chem. Phys.* **1987**, *86*, 866.

(37) Martin, J. M. L.; Sundermann, A. Correlation consistent valence basis sets for use with the Stuttgart-Dresden-Bonn relativistic effective core potentials: The atoms Ga-Kr and In-Xe. *J. Chem. Phys.* **2001**, *114*, 3408.

(38) Francl, M. M.; Pietro, W. J.; Hehre, W. J.; Binkley, J. S.; Gordon, M. S.; DeFrees, D. J.; Pople, J. A. Self consistent molecular orbital methods. XXIII. A polarization type basis set for second row elements. *J. Chem. Phys.* **1982**, *77*, 3654.

(39) Krishnan, R.; Binkley, J. S.; Seeger, R.; Pople, J. A. Self consistent molecular orbital methods. XX. A basis set for correlated wave functions. *J. Chem. Phys.* **1980**, *72*, 650.

(40) Enemark, J. H.; Feltham, R. D. Principles of structure, bonding, and reactivity for metal nitrosyl complexes. *Coord. Chem. Rev.* **1974**, *13*, 339.

(41) Matson, E. M.; Park, Y. J.; Fout, A. R. Facile Nitrite Reduction in a Non-heme Iron System: Formation of an Iron(III)-Oxo. *J. Am. Chem. Soc.* **2014**, *136*, 17398.

(42) Moore, C. M.; Szymczak, N. K. Nitrite reduction by copper through ligand-mediated proton and electron transfer. *Chem. Sci.* **2015**, *6*, 3373.

(43) Kwon, Y. M.; Delgado, M.; Zakharov, L. N.; Seda, T.; Gilbertson, J. D. Nitrite reduction by a pyridinediimine complex with a proton-responsive secondary coordination sphere. *Chem. Commun.* **2016**, *52*, 11016.

(44) Cioncoloni, G.; Roger, I.; Wheatley, P. S.; Wilson, C.; Morris, R. E.; Sproules, S.; Symes, M. D. Proton-Coupled Electron Transfer Enhances the Electrocatalytic Reduction of Nitrite to NO in a Bioinspired Copper Complex. *ACS Catal.* **2018**, *8*, 5070.

(45) Yi, J.; Thomas, L. M.; Richter-Addo, G. B. Distal Pocket Control of Nitrite Binding in Myoglobin. *Angew. Chem., Int. Ed.* **2012**, *51*, 3625.

DOI: 10.1021/acs.inorgchem.9b01274